Integration of Crosswind Forces into Train Dynamic Modelling

C Baker, H Hemida, S Iwnicki, G Xie and D Ongaro

Proceedings of the Institution of Mechanical Engineers, Part F: Journal of Rail and Rapid Transit 2011 225: 154
DOI: 10.1177/2041301710392476

Integration of crosswind forces into train dynamic modelling

C Baker[1], **H Hemida**[1]*, **S Iwnicki**[2], **G Xie**[2], and **D Ongaro**[2]
[1]Birmingham Centre for Railway Research and Education, School of Civil Engineering, University of Birmingham, Birmingham, UK
[2]Rail Technology Unit, Manchester Metropolitan University, Manchester, UK

The manuscript was received on 26 April 2010 and was accepted after revision for publication on 3 November 2010.

DOI: 10.1177/2041301710392476

Abstract: In this paper a new method is used to calculate unsteady wind loadings acting on a railway vehicle. The method takes input data from wind tunnel testing or from computational fluid dynamics simulations (one example of each is presented in this article), for aerodynamic force and moment coefficients and combines these with fluctuating wind velocity time histories and train speed to produce wind force time histories on the train. This method is fast and efficient and this has allowed the wind forces to be applied to a vehicle dynamics simulation for a long length of track.

Two typical vehicles (one passenger, one freight) have been modelled using the vehicle dynamics simulation package 'VAMPIRE®', which allows detailed modelling of the vehicle suspension and wheel–rail contact. The aerodynamic coefficients of the passenger train have been obtained from wind tunnel tests while those of the freight train have been obtained through fluid dynamic computations using large-eddy simulation. Wind loadings were calculated for the same vehicles for a range of average wind speeds and applied to the vehicle models using a user routine within the VAMPIRE package. Track irregularities measured by a track recording coach for a 40 km section of the main line route from London to King's Lynn were used as input to the vehicle simulations.

The simulated vehicle behaviour was assessed against two key indicators for derailment; the Y/Q ratio, which is an indicator of wheel climb derailment, and the $\Delta Q/Q$ value, which indicates wheel unloading and therefore potential roll over. The results show that vehicle derailment by either indicator is not predicted for either vehicle for any mean wind speed up to 20 m/s (with consequent gusts up to around 30 m/s). At a higher mean wind speed of 25 m/s derailment is predicted for the passenger vehicle and the unladen freight vehicle (but not for the laden freight vehicle).

Keywords: train aerodynamics, side winds, large-eddy simulation, train dynamics, VAMPIRE®

1 INTRODUCTION

The stability of high-speed trains in cross winds has become a major issue of concern in recent years and a considerable amount of work has been carried out in a number of countries around the world in this area – [**1**–**9**] for high-speed trains in the UK [**10**–**12**], for a European wide approach and [**13**] in Japan. In particular much recent work has been directed towards the development of a CEN (Comite' Europe'en de Normalisation) code of practice for vehicle acceptance, and the development of a suitable technical standards for interoperability (TSI) for train acceptance purposes [**14**, **15**]. The current methods for assessing cross wind stability are based on the use of wind tunnel or computational fluid dynamics (CFD) derived force and moment coefficients that are then used in multi-body dynamic simulations with specified onset wind conditions in order to predict specific levels of wheel unloading. Although this work has led to a consistent approach in the assessment of train acceptability, major assumptions have been made in this process. First, the specified methods do not

*Corresponding author: Birmingham Centre for Railway Research and Education, School of Civil Engineering, University of Birmingham, Birmingham B15 2TT, UK.
email: h.hemida@bham.ac.uk

require the simulation of track irregularities in the multi-body system simulations. There are, however, some indications that such effects may be significant [**16**]. Second, the wind simulation is often much simpler than would be the case in reality. In particular the deterministic 'Chinese hat' gust profile [**2**] is often used as specified in the TSI, which is only an approximation to real gust events. Other investigators have used more realistic wind fields (for example, see reference [**17**]) and systematic variations in output from the Chinese hat profile have been observed. Where real wind speed fields are simulated, then the calculations are carried out at least partly in the frequency domain and cannot account for either discrete track irregularities, or non-uniform winds [**17**–**19**].

Simulations of the dynamic behaviour of railway vehicles in response to realistic track irregularities include very detailed representation of the vehicle suspension and wheel–rail contact and have developed significantly in recent years. Dirk *et al.* [**20**] describes a work that looks at the overturning of vehicles mainly due to the lateral forces experienced during the passage through curves, and also due to a transient increase in cross wind speed, in a manner similar to the work presented by some of the present authors in reference [**7**]. It does not, however, consider fully turbulent cross winds as described in this article.

The latest versions of the established simulation tools such as VAMPIRE® and SIMPACK [**21**] allow long sections of track to be processed quickly even when non-linear models of suspension components and vehicle track interaction are included. This article considers these issues in some detail. The chief novelty of the approach is the modelling of realistic wind fields that can be used as input to dynamic models in which track irregularities and discontinuities are properly taken into account, using a time-domain approach. Real track data are used together with a generated time history of wind forces acting on the vehicle. This allows statistical post-processing of the data and assessment of potential derailment at specific locations. Although it is not expected that the methods outlined here can be used routinely in train acceptance calculations, they do give an insight into the physics of the problem that allows the limitations of the simpler methods to be understood more fully.

In section 2 an outline to the calculation method is given. Two sets of vehicle characteristics were used in the calculations – those for the Class 365 electric multiple unit(e.m.u.) and a freightliner flat with a 60 ft container (the latter type of vehicle having not been considered in great detail by previous investigations). Section 3 describes how the necessary aerodynamic force information was obtained for the two vehicles – wind tunnel tests for the Class 365 and large eddy simulation (LES) CFD calculations for the freight container and wagon. Section 4 then considers the simulation of the unsteady aerodynamic forces on the train and section 5 describes the integration of these forces into the program VAMPIRE and discusses the implications of the results that were obtained. Finally, some conclusions are drawn in section 6.

2 OUTLINE OF THE CALCULATION METHOD

The calculation method that will be used in this article has the following components.

1. The simulation of wind time series along a 37 km section of the track, using a calculation method that ensures that the time history of wind speed produced has the correct statistical behaviour.
2. The transformation of these wind time series into time series of wind velocity relative to the train, through a vector addition of wind speed and train speed.
3. The use of these wind time series to generate train force and moment time series. This requires knowledge of the train aerodynamic force and moment coefficients, and of the aerodynamic weighting functions that relate wind velocity fluctuations to force fluctuations.
4. The input of these force and moment time series into a VAMPIRE model of a train passing along the simulated track, with the track irregularities suitably modelled. (Note that the track irregularities are statistically independent of the simulated wind conditions. In the future, a more detailed statistical analysis will be carried out in which a range of different wind simulations will be used with a specific track irregularity profile.)
5. The investigation of the time histories of flange climbing and wheel unloading for a variety of wind speeds and train speeds.

2.1 Calculation of wind loadings

Steps 1–3 are fully discussed in a recent article by one of the authors [**4**], and only a brief outline is given in what follows. The wind velocity is calculated from the sum of its mean ($\bar{u}$) and fluctuating component (u'). The mean velocity component is specified in the calculations and, in what follows, is assumed to be normal to the track. The fluctuating component is simulated as a series of superimposed sine waves. The required amplitudes, frequencies, and phases of these sine waves are calculated from the wind spectrum 'seen' by a moving vehicle outlined in reference [**22**]. This method ensures that the calculated wind time series has the correct spectral and correlation characteristics and is representative of real conditions. The calculations have been carried out for a turbulence intensity of 0.15 and a turbulence length scale of 50 m, which are representative of rural terrain roughness conditions, close to ground level.

The time histories of wind speed relative to the train, with a mean value of V and a fluctuating value of V' are then calculated from the simple vector addition

$$\bar{V} + V' = (v^2 + (\bar{u} + u')^2)^{0.5}$$

where v is the train velocity. The aerodynamic force on the train F (which represents either the side force S or the lift force L acting at the centre of pressure of the vehicle) is then given by the sum of the mean and fluctuating forces, which are in turn given by

$$\bar{F} = 0.5\rho A C_F(\Psi)\bar{V}^2$$

$$F' = \rho A C_F(\Psi)\bar{V}V'$$

where the velocity-squared terms have been ignored. $C_F(\Psi)$ is either the side or the lift force coefficient and is a function of Ψ, the mean yaw angle – the angle between the train direction of travel and the mean velocity vector. ρ is the density of air and A is a reference train area. Baker [**4**] further shows that the fluctuating component of force can be written as

$$F' = \rho A C_F \bar{u}\left(1 + \frac{1}{2C_F}\frac{\mathrm{d}C_F}{\mathrm{d}\Psi}\cot\Psi\right)\int_0^\infty h_F(\tau)u'(t-\tau)\,\mathrm{d}\tau$$

Here $h_F(\tau)$ is the aerodynamic weighting function for either side force or lift force, which relates the fluctuating wind velocity to the fluctuating force. Baker [**4**] shows that to a good approximation, this can be given by

$$\bar{h}_F = (2\pi\overline{n'})^2\bar{\tau}\mathrm{e}^{-2\pi\overline{n'}\bar{\tau}}$$

$\bar{\tau}$ is a dimensionless time and $\bar{h}_F$ is a dimensionless weighting function, with the non-dimensionalization being with $\bar{V}$ and the vehicle length L . The parameter $\bar{n'}$ was shown to be approximated by

$$\overline{n'} = \gamma \sin\Psi$$

where γ has the value of 2.5 for side force and 2.0 for lift force. The weighting function is effectively a filter on the wind conditions that allows for the fact that the overall forces on the vehicle are an integration of the fluctuating forces over the vehicle surface which are not fully correlated, which results in the forces at a particular time being a function of the wind velocity over a short time period before that.

It has been noted in the previous full-scale and wind tunnel experiments [**3**, **4**] that the side and lift force time histories are only well correlated over relatively long time periods (2–4 s and above), but for shorter time periods there is little correlation between the two time series. This is no doubt due to small-scale atmospheric turbulence having different effects on the side and lift force fluctuations. To allow for this, the method of Baker [**4**] calculates the side and lift force coefficient time series from the same wind time series for frequencies of less than 0.25 Hz, thus resulting in perfect correlation between the time series for periods greater than 4 s, with uncorrelated time series being used for the higher frequency range, thus resulting in no side/lift force correlations in this frequency range.

2.2 Simulation of vehicle dynamic behaviour

Vehicle models have been set up in the vehicle dynamics simulation package – VAMPIRE – to represent a typical E.M.U. passenger vehicle and a freight wagon loaded with containers. VAMPIRE allows a detailed description of the vehicle suspension including non-linearities, input of measured track irregularities and detailed non-linear modelling of the wheel–rail contact. Outputs from the VAMPIRE simulation can include wheel–rail forces, position of the contact between the wheel and the rail, and behaviour of the vehicle bodies. Wind loadings were applied to the vehicle main body (or the container body in the case of the freight vehicle) using a user routine written in Simulink.

Further details for each vehicle model are given below.

2.2.1 Class 365 E.M.U

The Class 365 is a typical multiple unit with a maximum speed of 100 mile/h (161 km/h) (see Fig. 1). The tare weight is 34 tons giving an axle load of 8.5 tons, and the wheel diameter is 0.84 m. The vehicle model in VAMPIRE consisted of seven bodies with a total of 38 degrees of freedom; four wheelsets each with five degrees of freedom, and two bogies and the main body with six degrees of freedom each. The suspension was modelled with shear springs and viscous dampers and non-linear elements representing bump stops and air springs.

The wheel–rail contact was modelled using a pre-computed geometry table using new P8 wheel profiles running on BS113 rail. Normal wheel–rail forces are calculated at each time step using Hertz theory and the pre-calculated geometry. Tangential wheel–rail forces are calculated using Kalker's FASTSIM routine within VAMPIRE.

2.2.2 Freight wagon

The freight wagon modelled is a flat bed container wagon (Fig. 2). The tare weight is 20 tons and the laden weight is 80 tons. The maximum speed in the tare condition is 75 mile/h (120.7 km/h) falling to 60 mile/h (96.6 km/h) for the laden condition. To allow the worst-case wind loading to be included the tare vehicle was considered to have all containers in place, but empty. The vehicle model in VAMPIRE consisted of 12 masses with a total of 68 degrees of freedom. In addition to the wheelsets and bogies, the main body is split into a forward reaction and a rear section to allow twist

Fig. 1 Class 365 passenger vehicle (photo Tony Miles)

Fig. 2 Flat bed container vehicle (photo Tony Miles)

to be investigated and there are additional bodies to represent the side bearers. Forty-two friction elements with varying normal force according to vertical load were used to represent the sliding friction in the Lenoir links that make up the Y25 suspension. The torsional stiffness of the wagon frame was included in the simulation model although this did not seem to have a significant effect on the results for the cases run.

Wheel–rail contact was modelled as with the passenger vehicle, except that a P10 wheel profile was used for the geometry calculations.

2.2.3 *Integration of aerodynamic forces into simulation*

The calculated wind forces as described in section 2 are applied at the car body centre of gravity. Only side forces and lift forces are simulated, with no simulation of rolling moments. Such an approach effectively assumes that the centre of pressure is at the car body centre of gravity. Although a number of previous investigations suggest that this is a reasonable approximation (such as those outlined in reference

[**1**]), it must be admitted that this has not been verified for the vehicles under consideration. These data are provided at 0.05 s intervals but due to the high volume of data a Simulink routine was set up to take the data and input it into the VAMPIRE simulation as required. The wind was applied separately from both sides of the vehicle to allow the worst case to be considered.

The wind speed cases applied were 0 (the reference case), 10, 17 and 25 m/s at the height of the vehicle. These values are all mean wind speeds, with the simulated gust speeds being around 50 per cent higher in all cases. These values were chosen to represent a range of scenarios – a mean wind speed of 10 m/s being conventionally regarded as the lower limit of 'strong' winds, with a mean wind speed of 25 m/s (and thus, depending on terrain types), a gust speed of 35–40 m/s being around the 1-in-50-year value at many sites.

2.2.4 Track data

Various scenarios of combination of wind speed and vehicle speed with vehicles running in cant deficiency and cant excess have been carried out during this project and showed that the worst cases were on higher speed (and therefore larger radius) curves with cant deficiency and the wind force acting towards the outside of the curve. For this reason the track used for this study was selected to include high line speed and shallow curves. The simulations were carried out with perfect track (no irregularities) as well as real track from recording coach measurements. The track data were provided by Network Rail for the track from King's Cross Station in London to King's Lynn in Cambridgeshire. A 36.5 km section of this track was used for the simulations and data for the cross level, curvature, lateral alignment, vertical alignment, and gauge irregularities input to the vehicle dynamics model every 0.2 m. A sample of these data is shown in Fig. 3.

2.3 Assessment of vehicle behaviour

Two key indicators are often used in the assessment of the likelihood of derailment of a railway vehicle. The first of these is the ratio of the lateral force to the vertical force at any wheel, known as Y/Q or L/V or the 'derailment quotient'. As the lateral force increases the potential for flange climbing where the wheel rides up the flange onto the rail head is increased, conversely an increase in the vertical force at this wheel reduces this possibility. Both of these factors are included in the derailment quotient and a limit can be calculated based on the coefficient of friction and flange angle using a simple method first outlined by Nadal and described by Gilchrist and Brickle [**23**]. The practical limit for the derailment quotient in most cases is between 1 and 1.2. The second derailment indicator relates to roll over of the vehicle and is the level of wheel unloading at any wheel. This is normally defined as the ratio of actual load to static load at the wheel or $\Delta Q/Q$ and can be easily calculated during a vehicle

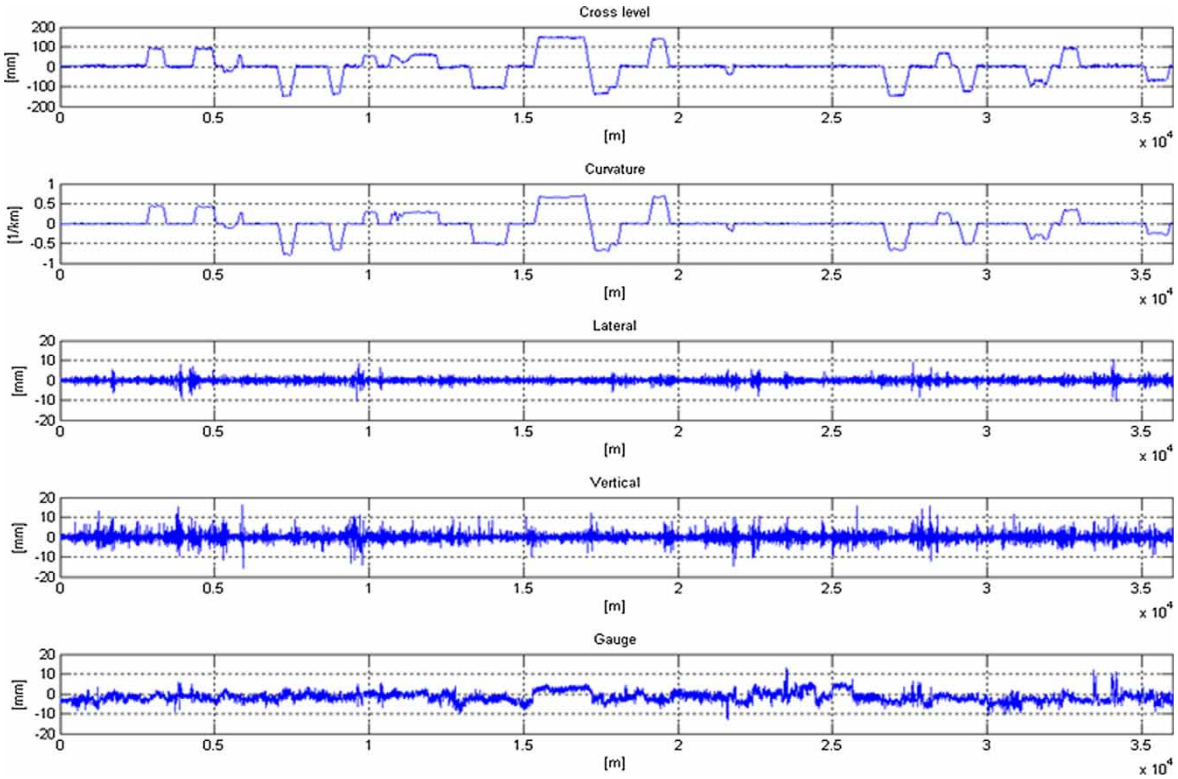

Fig. 3 Track data for the route used in the simulation

dynamics simulation. A limit for this value is set at 0.1 (i.e. 90 per cent unloading) by the TSI [**15**]. In line with normal practice, the simulations values are filtered by the application of a 2 m moving window to remove peaks of very short duration which will not result in derailment.

Preliminary work in this project indicated that the $\Delta Q/Q$ limit was usually reached well before the Y/Q limit under typical vehicle operation and wind loading conditions [**24**].

3 DETERMINATION OF AERODYNAMIC PARAMETERS

3.1 Class 365

The aerodynamic force and moment coefficients for the Class 365 e.m.u. were obtained from a series of wind tunnel tests that were carried as part of a project to look at the sway of pantographs relative to the overhead wire system. These wind tunnel tests are fully reported in references [**3**] and [**4**] and the pantograph sway issue more fully discussed in reference [**4**]. The tests were carried out with a 1/30th scale model of the vehicle mounted within a wind tunnel in which a rural atmospheric boundary layer had been simulated (Fig. 4). Full details of the simulation are given in reference [**3**]. The shear and the turbulence levels and length scales simulated were consistent with those that would be expected from a relatively smooth rural environment. Pressures were measured at a large number of points over the surface of the vehicle using multi-channel transducers, and the overall steady and unsteady forces were calculated from an area integration of the pressure field. In particular, side and lift forces were calculated, and side and lift force coefficients formed. The reference area A used in the formation of the force coefficients was 0.0061 m^2, this being the side area of the vehicle at model scale. The measured side and lift force coefficients are shown in Fig. 5 as a function of yaw angle – the angle between the train direction of travel and the wind vector relative to the train. The method outlined in reference [**4**] assumes that the force coefficients can be represented by sine curves, and thus fully specified by a representative value at 90°. Although such an approach is not absolutely necessary, it is analytically convenient and of sufficient accuracy for the illustrative results presented here. For the side force coefficient, the 90° value was taken as 1.15, while for the lift force coefficient, the value was taken as 0.8, which gives the best fit to the data over the yaw angle range of most interest (20–30°). These tests were also used to obtain values of the aerodynamic weighting function. The method is described in detail in reference [**4**], but essentially uses

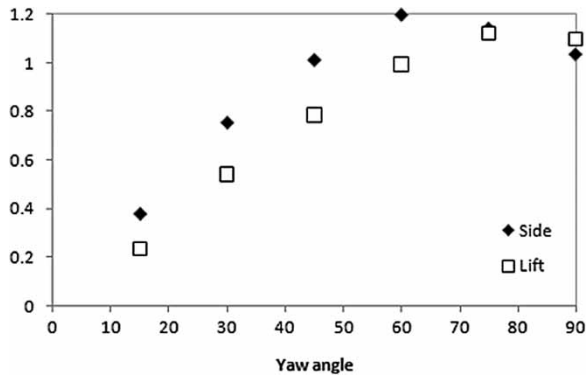

Fig. 5 Ensemble averaged of the aerodynamic side and lift force coefficients on the Class 365 e.m.u.

Fig. 4 Class 365 e.m.u.

measurements of the force and wind spectra to form the aerodynamic admittance for side and lift forces. The weighting function is then the Fourier transform of this admittance.

3.2 Freight vehicle

For the container vehicle, the force and moment coefficients were obtained from LES CFD calculations. The model used in our computation is a 1/20 scale single-stacked wagon at the middle of a row of similar wagons representing a freight train. The wagon consists of two parts: freightliner and container. The freightliner is shown in Fig. 6, which is a simplified version of the real freightliner flat. The freightliner model consists of two simple bars, with thickness 1 cm each, and bogies. The bogies are modelled as boxes attached to the bottom of the two bars. The freightliner length and width are 1 and 0.1 m, respectively. The container is a simple box mounted on the top of the freightliner, as shown in Fig. 6. The length, height, and width of the container are 0.9, 0.1, and 0.125 m, respectively. The height of the container from the ground, H in Fig. 3, is 0.179 m. The area A used in the definition of the force coefficients is defined as the side area of the carriage, based on the height of the carriage from the ground and the length of the carriage, that is, $A = 0.179\,\mathrm{m}^2$.

The flow around a moving train is very complicated and consists of large range of turbulent scales. The wake flow and boundary layer are usually dominated by large turbulent structures. Hence, a simulation method that resolves the large structures such as LES is preferable for simulations of the flow around trains. Generally, LES decomposes the structures of the flow into large and small scales. The large motions of the flow are directly simulated while the influence of small-scale motions on large-scale motions is modelled. LES has already been proved to be a reliable technique in the prediction of the flow around simplified trains and bluff bodies [**10**–**12**]. In the present work, LES using the standard Smagorinsky sub-grid scale model with model constant $C_S = 0.1$ is used. Four different LES calculations have been performed at four different side wind yaw angles: 15°, 30°, 60°, and 90°. The LES equations were discretized using a three-dimensional finite-volume method in a collocated grid arrangement. The commercial package ANSYS CFX has been employed to solve the LES equations. To investigate the influence of the mesh resolution on the results and to establish numerical accuracy, three computations were made on three different computational grids: coarse, medium, and fine. The coarse mesh consists of 3 million nodes, whereas the medium and fine meshes consist of 5 and 7 million nodes, respectively. The ICEM-CFD mesh generator package is employed to build the structured meshes around the wagon. An O-type mesh was made in a belt of thickness of $0.1H$ around the container followed by a C-type grid with a thickness of about $0.5H$. More than half the total number of nodes is in the O- and C-type grids. H-type grid topology is used in the rest of the computational domain. This allows the generation of a smooth mesh in all directions. To resolve the boundary layer on the model surface and to capture the variation of the flow physics around it, the mesh is concentrated around the model where more than 30 per cent of the total nodes are confined in the O- and C-type grids. This ensured that the value of the wall normal resolution, y^+, is below 5, 1.5, and 0.9 for the coarse, medium, and fine meshes, respectively. The governing equations are solved all the way to the model wall to ensure proper variation of the flow quantities in the near-wall region, where much of the flow physics originates. A constant time step of 1.0×10^{-4} s. is used throughout the entire simulation. This gives a maximum Courant–Friedrichs–Lewy (CFL) number of about 1.0 and its root mean square value of about 0.6. Good agreement has been obtained between the results of the medium and fine meshes. The trends of our LES results are in agreement with the experiments of Alam and Watkins [**25**] that has been collected on a freight train with a double stacked container.

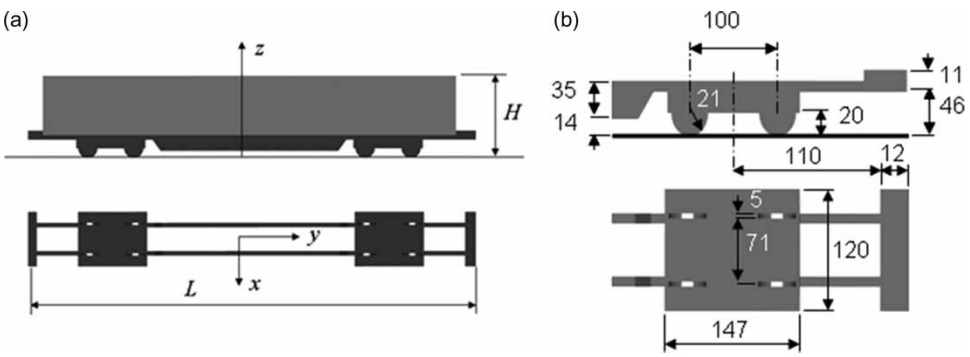

Fig. 6 (a) Simplified freight wagon geometry: bottom freightliner and top freight wagon. (b) Dimensions of the freightliner in mm

The obtained instantaneous velocity field from LES has been used to visualize the flow structures around the wagon, as shown in Fig. 7. The instantaneous surface pressure and shear stress have been used to calculate the aerodynamic side force and lift force coefficients. The time-averaged values of these coefficients are shown in Fig. 8.

The method outlined in reference [**4**] assumes that the force coefficients can be represented by sine curves, and thus fully specified by a representative value, 90°. It can be seen from Fig. 8 that a sine curve would not be a good fit for the freight container data over the complete yaw angle range. Values of the representative 90° coefficients were thus chosen such that there was a reasonable fit over the angle range of around 15–45° which is of most relevance to the calculations presented here – 1.256 for a side force coefficient and 0.874 for a lift force coefficient. In addition the assumed values of the aerodynamic weighting function were assumed to have the same form as for the Class 365 e.m.u., which is a major assumption that requires fuller verification.

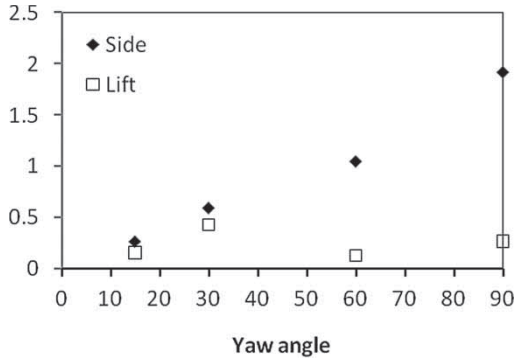

Fig. 8 Time-averaged aerodynamic force coefficients obtained from the LES on the freight wagon

4 CALCULATION OF FORCE TIME HISTORIES

Figure 9 shows an example of a simulated wind field, both relative to the track and relative to the train for a wind speed of 20 m/s and a train speed of 40 m/s. The effect of the vectorial addition of wind speed and vehicle speed can be clearly seen, with a relatively lower fluctuating component of the wind speed relative to the vehicle. The calculated side and lift force coefficient time histories for this situation (for the Class 365 in this case) are then shown in Fig. 10.

The large scale of the fluctuating forces in Fig. 10 may appear surprising in view of the relatively small-scale velocity fluctuations relative to the vehicle in Fig. 9. However, a consideration of the expression for fluctuating forces in section 2.1 shows that the fluctuations are significantly magnified at low yaw angles by the multiplier $(1 + (1/2C_F)(dC_F/d\Psi)\cot\Psi)$, which Baker [**4**] shows is a result of the application of static wind tunnel data to the moving vehicle situation – in essence longitudinal velocity fluctuations also cause significant yaw angle fluctuations, which can, at yaw angles such as considered here, prove to be quite significant. These large fluctuations due to yaw angle changes have only recently been appreciated in reference [**4**], and are included here for the first time.

5 CALCULATION OF VEHICLE RESPONSE

As previously discussed, the most useful indicator of derailment has been shown to be the rollover indicator, $\Delta Q/Q$. Simulations of $\Delta Q/Q$ were therefore carried out for both passenger and freight vehicles running at full speed on the selected track and with the wind force applied as described and with the following results.

5.1 Class 365

Simulations were completed for all wind speeds without the derailment quotient exceeding the limit value.

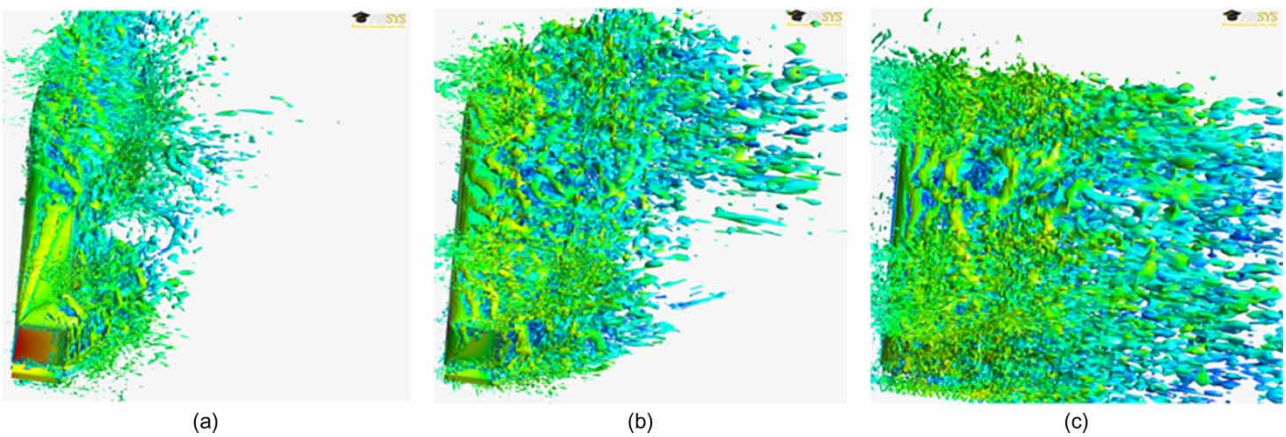

Fig. 7 Instantaneous flow structures: (a) 30° yaw angle; (b) 60° yaw angle; and (c) 90° yaw angle

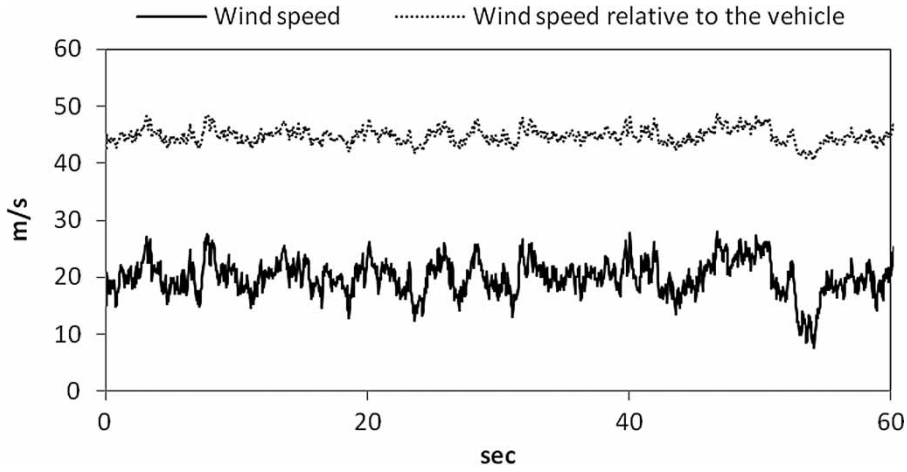

Fig. 9 A typical simulated wind field

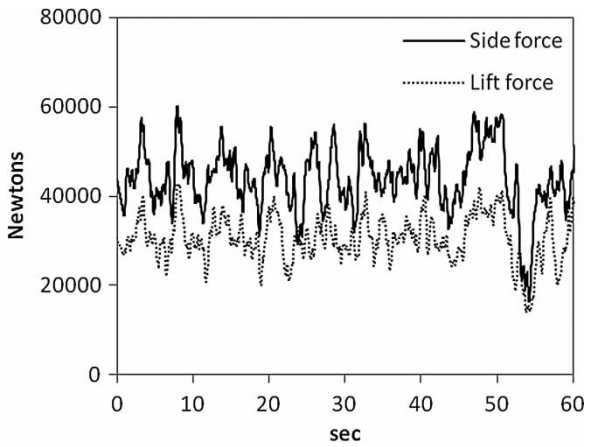

Fig. 10 Aerodynamic side and lift forces calculated from the wind field in Fig. 9

Figure 11 shows the $\Delta Q/Q$ values for the left wheel on the leading axle for all wind speeds and the maximum vehicle speed of 100 mile/h (161 km/h). $\Delta Q/Q$ is seen to increase with wind speed and for the 25 m/s wind speed the $\Delta Q/Q$ value exceeds the limit value of 0.9 frequently.

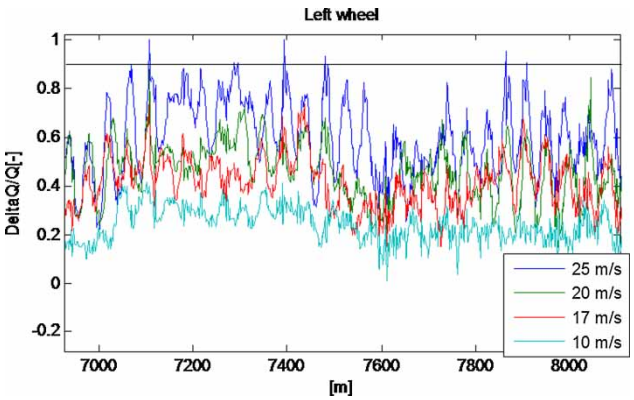

Fig. 11 Time history of $\Delta Q/Q$ for the passenger vehicle

The probability distribution of $\Delta Q/Q$ at the left leading wheel for the whole route under different wind speeds is presented in Fig. 12 . As wind speed increases, the aerodynamics increase the chance of wheel unloading. These results show that for a mean wind speed of 25 m/s (with gust speeds around 50 per cent higher) there is a significant number of exceedences of the 0.9 limit.

Comparisons of the distributions of $\Delta Q/Q$ were also made between the artificial perfect track and real track, with measured irregularities as shown in Fig. 13. At a lower wind speed, the value of $\Delta Q/Q$ is predominately around 0.2 with and without track irregularities which only have the effect of spreading out the distribution of $\Delta Q/Q$. As the wind speed increases, this effect becomes smaller and there is almost no difference between the perfect and real track for the wind speed of 25 m/s. At higher wind speeds the vehicle accelerations are dominated by the wind forces and the effect of track irregularities becomes less significant.

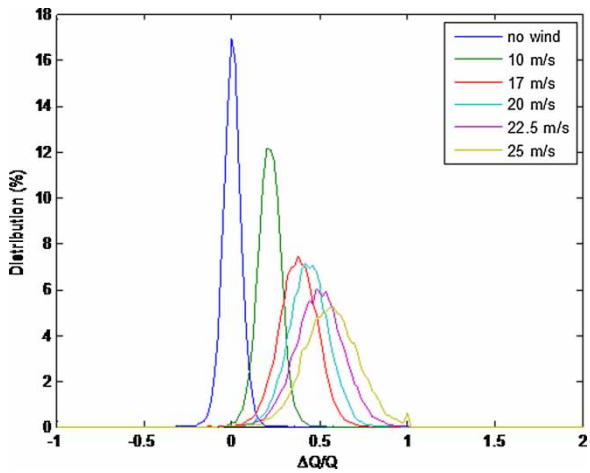

Fig. 12 Probability distribution of $\Delta Q/Q$ for passenger vehicle at different wind speeds

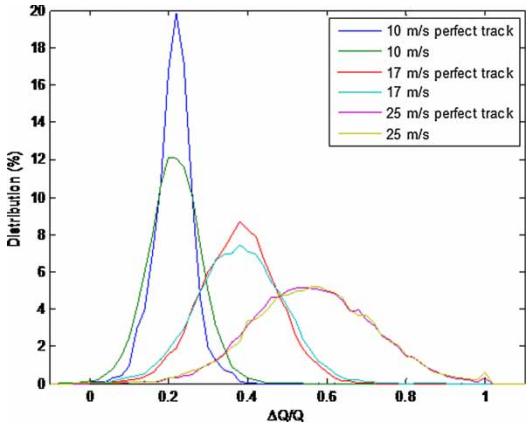

Fig. 13 Probability distribution of $\Delta Q/Q$ for passenger with and without track irregularities

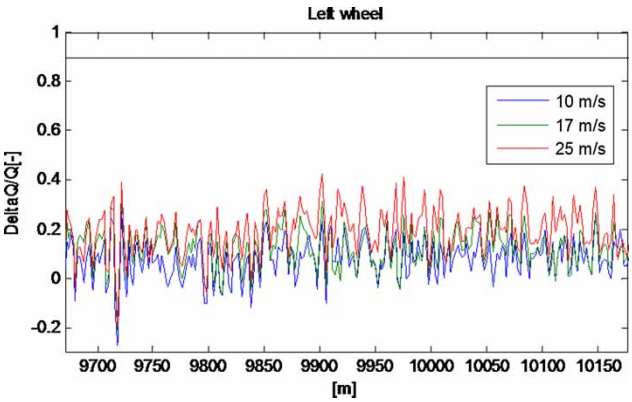

Fig. 14 $\Delta Q/Q$ for the laden vehicle under three wind speed forces from the left side

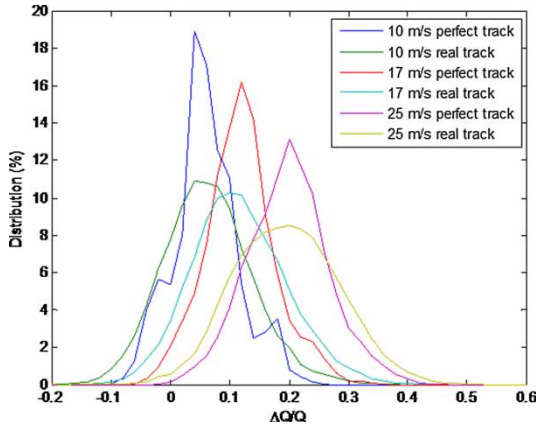

Fig. 15 Probability distribution of $\Delta Q/Q$ for the laden vehicle compared between the perfect and real track under different wind speeds

5.2 Freight vehicle

VAMPIRE simulations were carried out for three wind speeds: 10, 17, and 25 m/s. For the case of the laden vehicle, Y/Q and $\Delta Q/Q$ were very low for all wind speeds and no derailment risk was found (Fig. 14). In comparing the results between the perfect and real track, it is again found that the track irregularity has

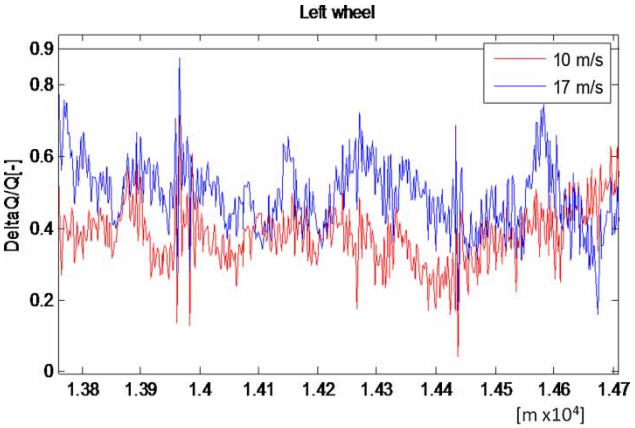

Fig. 16 $\Delta Q/Q$ for the tare vehicle under forces from wind speeds of 10 and 17 m/s

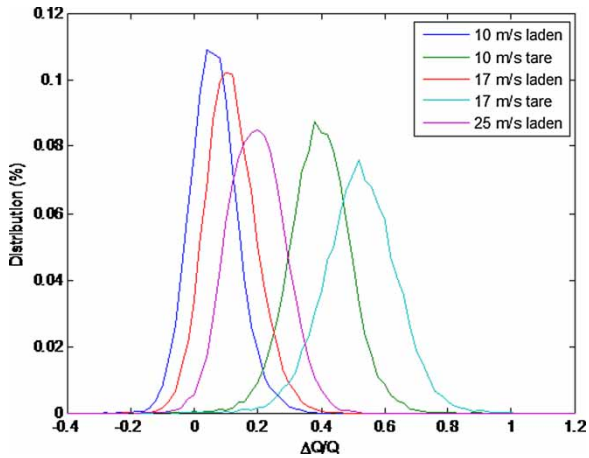

Fig. 17 Comparison of $\Delta Q/Q$ between the tare and laden vehicle under different wind speeds

the effect of spreading the distribution of $\Delta Q/Q$ for all three wind speeds (Fig. 15).

For the case of the tare vehicle, VAMPIRE simulations were completed for wind speeds of 10 and 17 m/s but complete wheel unloading occurred for the wind speed of 25 m/s and the simulation was stopped. $\Delta Q/Q$ also exceeded the limit value at some locations at a wind speed of 17 m/s, as shown in Fig. 16. The comparison between the tare and laden vehicle is presented in Fig. 17.

6 CONCLUSIONS

A new method of deriving wind loading forces has been tested for a railway vehicle travelling at speed through an unsteady wind.

These wind loadings have been evaluated from wind tunnel tests and from computational fluid dynamic simulations and applied to vehicle dynamics models for two typical UK vehicles. All relevant suspension properties and wheel–rail contact forces have been

included, and measured track data from a section of UK main line were used as an input to the simulations.

Flange-climb derailment and wheel unloading have been used as assessment criteria for the simulation outputs and the results of the simulations show that for all average wind speeds up to 20 m/s and all realistic vehicle speeds no derailment of the passenger vehicle or the freight vehicle are predicted. This is reassuring but perhaps not surprising as experience shows that the vehicles modelled do in practice operate safely in the highest wind conditions currently experienced.

At an extreme average wind speed of 25 m/s with the vehicle operating at the maximum line speed derailment is predicted for the passenger vehicle and the freight vehicle in its tare condition. The usefulness of this technique will therefore be in extending current practice to situations outside the current normal range of experience where lighter or faster vehicles may be envisaged or if average wind speeds or gust speeds increase in the future.

ACKNOWLEDGEMENTS

The authors are grateful to the Engineering and Physical Sciences Research Council (EPSRC) for supporting this project through Rail Research UK (RRUK).

REFERENCES

1 **Baker, C., Cheli, F., Orellano, A., Paradot, N., Proppe, C.,** and **Rocchi, D.** Cross wind effects on road and rail vehicles. *Veh. Syst. Dyn.*, 2009, **47**(8), 983–1022 (invited paper).

2 **Quinn, A. D.** and **Baker, C. J.** Spatial and temporal correlations of wind speeds. *Proc. Inst. Civil Engng Struct. Build.*, 2010, **163**, 65–72.

3 **Baker, C. J.** and **Sterling, M.** Aerodynamic forces on multiple unit trains in cross winds. *J. Fluids Engng*, 2009, **131**, 101103-1.

4 **Baker, C. J.** The simulation of unsteady aerodynamic cross wind forces on trains. *J. Wind Engng Ind. Aerodyn.*, 2010, **98**(2), 88–99.

5 **Bouferrouk, A., Baker, C. J., Sterling, M., O'Neil, H.,** and **Wood, S.** *Calculation of the cross wind displacement of pantographs, bluff body aerodynamics and its applications*, 2008 (Milano, Italy).

6 **Baker, C. J.** The effect of unsteady crosswind forces on train dynamic behaviour. In Proceedings of the 5th European and African Conference on *Wind engineering*, Florence, 2009.

7 **Baker, C. J., Bouferrouk, A., Perez, J.,** and **Iwnicki, S. D.** The integration of cross wind forces into train dynamic calculations. In Proceedings of the World Congress on *Rail research*, Seoul, South Korea, 2009.

8 **Baker, C. J., Sterling, M., Bouferrouk, A., O'Neil, H., Wood, S.,** and **Crosbie, E.** *Aerodynamic forces on multiple unit trains in cross winds. Bluff body aerodynamics and its applications*, 2008 (Milano, Italy).

9 **Baker, C. J., Lopez-Calleja, F., Jones, J.,** and **Munday, J.** Measurements of the cross wind forces on trains. *J. Wind Engng Ind. Aerodyn.*, 2004, **92**, 547–563.

10 **Hemida, H.** and **Krajnovic, S.** LES study of the influence of the nose shape and yaw angles on flow structures around trains. *J. Wind Engng Ind. Aerodyn.*, 2010, **98**(1), 34–46.

11 **Hemida, H.** and **Krajnovic, S.** Exploring flow structures around a simplified ICE2 train subjected to a 30° side wind using LES. *J. Engng Appl. Comput. Fluid Mech.*, 2009, **3**(1), 28–41.

12 **Hemida, H.** and **Krajnovic, S.** LES Study of the Influence of a train-nose shape on the flow structures under the influence of a cross-wind. *J. Fluid Engng*, 2009, **130**(9), 091101.

13 **Fujii, T., Maeda, T., Ishida, H., Imai, T., Tanemoto, K.,** and **Suzuki, M.** Wind induced accidents of train vehicles and their measures in Japan. *Q. J. RTRI Jpn.* 1999, **40**(1), 50–55.

14 CEN. Railway applications – aerodynamics – part 6: requirements and test procedures for cross wind assessment, EN 14067-6, 2010.

15 TSI. Technical specification for interoperability of high speed rolling stock (TSI HS RST), Official Journal of the European Union, L64 of 7/3/2008.

16 **Iwnicki. S. D.** Simulation of wheel–rail contact forces, *Fatigue Fract. Engng Mater. Struct.*, 2003, **26**, 887–900.

17 **Cheli, F., Corradi, R., Diana, G., Ripamonti, F., Rocchi, D.,** and **Tomasini, G.** Methodologies for assessing trains CWC through time-domain multibody simulations. In Proceedings of the 12th International Conference on *Wind engineering*, Cairns, Australia, 2007.

18 **Cheli, F., Corradi, R., Diana, G.,** and **Tomasini, G.** A numerical experimental approach to evaluate the aerodynamic effects on rail vehicle dynamics. *Veh. Syst. Dyn.*, 2006, **44**, 791–804.

19 **Cheli, F., Corradi, R., Diana, G., Tomasini, G., Roberti, R.,** and **Cheli, R.** Cross wind aerodynamic forces on rail vehicles – part II. Numerical model for vehicle dynamic response computation. In Proceedings of the World Congress on *Railway research*, Edinburgh, 2003.

20 **Dirk, T., Mats, B.,** and **Sebastian, S.** Measurements and simulations of rail vehicle dynamics with respect to overturning risk. *Veh. Syst. Dyn.*, 2010, **48**(1), 97–112.

21 **Iwnicki, S. D.** *The Manchester benchmarks for rail vehicle simulation*, 1999 (Swets & Zeitlinger B.V., Lisse).

22 **Cooper, R. K.** Atmospheric turbulence with respect to moving ground vehicles. *J. Wind Engng Ind. Aerodyn.*, 1985, **17**, 215–238.

23 **Gilchrist A. O.** and **Brickle B. V.** A re-examination of the proneness to derailment of a railway wheelset. *J. Mech. Sci.*, 1976, **18**(3), 131–141.

24 **Baker, C. J., Bouferrouk, A., Perez, J.,** and **Iwnicki, S. D.** The integration of cross wind forces into train dynamic calculations. In Proceedings of the World Congress on *Railway research*, Edinburgh, 2003.

25 **Alam, F.** and **Watkins, S.** Lateral stability of double stacked container wagon under crosswinds. In Proceedings of the International Conference on *Mechanical engineering (ICME2007)*, Dhaka, Bangladesh, 2007.